Performance Analysis of Hybrid FSO/RF Empowered V2N Communications with Multiple Relay Units

Neha Payal[1], Devendra Singh Gurjar[1], Suneel Yadav[2], and Radhika Gour[2]

***Abstract*— This paper considers mixed radio frequency (RF) and hybrid free space optics (FSO)/RF communications for information transfer between vehicles and the network where multiple infrastructures nodes, such as street lights, traffic lights, signboards, etc., act as relay units. Vehicles communicate with nearby infrastructure nodes in the first transmission phase using an RF link. In the next phase, an infrastructure node corresponding to the maximum signal-to-noise ratio (SNR) is selected to forward the signal to the base station using a hybrid FSO/RF link. An RF link is used as a backup connection to increase the system's reliability. To get practical insights, atmospheric turbulence-induced fading, pointing errors, and atmospheric attenuation, which may affect the FSO link's performance, are considered. In addition, the base station is deployed with multiple antennas. It exploits maximum-ratio combining when the RF link is active to improve end-to-end system performance. We derive closed-form expressions for the outage probability and system throughput to analyze the system's performance. We include the simulation results to verify that all the derived analytical findings are accurate.**

I. Introduction

In recent years, road accidents and traffic congestion have increased due to rapid urbanization and the increased mobility of urban dwellers. With the increase of vehicles in everyday lives, the requirement for coordinated vehicular interaction and safe transportation seems inescapable [1]. Vehicle-to-everything (V2X) communication has been introduced as a potential solution to alleviate these recently emerged demands. Specifically, V2X communications can provide improved safety applications, passenger alerts, vehicle traffic optimization, and present vehicle-sensing capabilities. Moreover, V2X communications are expected to be able to support a variety of cases, including optimal speed warnings, queue warnings, parking discovery, and do not pass warnings, all of which may improve transportation effectiveness and reduction in road accidents while also enhancing road safety [2], [3], [4]. By exchanging messages with infrastructure, automobiles, and pedestrians via appropriate wireless communication protocols, e.g., dedicated short-range communications (DSRC) and cellular network technologies, V2X communications can support diverse use cases.

The conventional approaches of spectrum re-structuring and cell densification still need to adequately address the demands of emerging wireless technologies and applications, requiring higher data rates. Optical wireless communications (OWC) may be a feasible solution to overcome these higher data rate requirements [5]. Depending on the carrier, OWC can be realized as free space optics (FSO), ultraviolet communications, or visible light communications. Recently, the benefits of a free license spectrum, high bandwidth, low installation cost with faster deployment, robust security, etc., have sparked much interest in FSO communication in academics and industry [6]. Even though FSO communication needs a line-of-sight (LoS) path between the transmitter and receiver, it is preferable for many practical applications due to its intrinsic benefits, such as higher bandwidth and excellent attainable data rates [7]. Moreover, FSO communication is a potential technique for delivering high-capacity wireless backhaul connectivity in sixth-generation [8]. Despite several advantages, atmospheric conditions such as atmospheric turbulence, misalignment errors, and attenuation and physical obstacles, including building barriers, fog, and earthquakes, can degrade or interrupt communication reliability. To increase the reliability of FSO communication, several efforts have been made in developing a hybrid FSO/radio-frequency (RF) system where an additional RF subsystem can be used as an alternative to the FSO subsystem as FSO and RF channels exhibit complementary characteristics [9], [10], [11]. Further, relaying techniques can be employed in RF-FSO networks to improve coverage and mitigate the impact of atmospheric turbulence and attenuation due to fog. Multiple relays can be prominently placed to expand the coverage area and ensure reliable communication even in the worst weather conditions [12].

In recent years, relay-assisted hybrid RF/FSO networks have been well studied in the literature [13], [14], [15], [16], [17], [18]. Specifically, in [13], the authors characterized the RF channel as Nakagami-m fading distribution and FSO link as Gamma-Gamma distribution to examine the outage probability (OP) and bit error rate (BER) of hybrid FSO/RF network. In [14], the authors investigated an FSO/RF network by taking into account generalized distributions, particularly $\alpha - \eta - k - \mu$ and Malaga distributions for RF and FSO channels, respectively. In [15], the authors derived a closed form OP expression for a relaying-based RF-FSO system. In [16], amplify-and-forward (AF) relaying with a hybrid RF/FSO system was presented, and the OP expression was derived by considering Nakagami-m and Gamma-Gamma distributed channels with turbulence and pointing error. In [17], the authors studied the performance of multi-user relay-assisted hybrid FSO/RF systems in terms of OP and BER. Whereas in [18], the OP and diversity order were studied for FSO/RF system by considering the decode-and-forward (DF) relaying with a nonlinear energy harvesting. However, the nodes were assumed to be stationary in the aforementioned works. The works in [19] and [20] used a first-order autoregressive method to define the mobility aspect of vehicles in such complex systems.

[1]N. Payal and D. S. Gurjar are with the Department of ECE, National Institute of Technology Silchar, Assam, 788010, India {neha21_rs, dsgurjar}@ece.nits.ac.in

[2]S. Yadav and R. Gour are with the Department of ECE, Indian Institute of Information Technology Allahabad, Prayagraj, 211015, India {suneel, radhika}@iiita.ac.in

979-8-3503-0219-6/23/$31.00 ©2023 IEEE

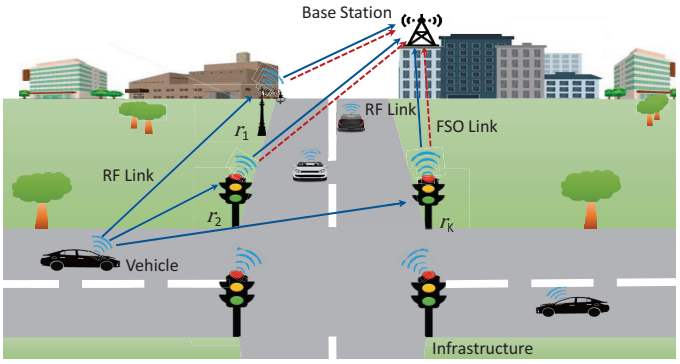

Fig. 1. Hybrid FSO/RF communication with multiple relay units.

Despite the fact that FSO communication systems have high data rates and low latency, their performance may be significantly constrained if operated as standalone systems due to the need for LoS and atmospheric turbulence. Motivated by the earlier efforts and highlighted difficulties, this work studies the performance of a hybrid FSO/RF system with multiple relay units. Here, in the first transmission phase, an RF link is used to enable communication between vehicles and multiple infrastructure nodes, whereas, in the next transmission phase, communication between infrastructures and a base station is enabled using a hybrid FSO/RF system. Vehicles and roadside units are deployed with single antenna devices, and the base station has multiple antennas. RF link assists the FSO link in reducing atmospheric turbulence effects, whereas multiple antennas installed at the base station enhance the system performance, resulting in a more reliable system. Further, DF-based relaying is used at relaying infrastructure nodes to provide relay cooperation. The relay node with better signal-to-noise ratio (SNR) is selected to transmit the signal to the base station. The channels are considered to be time-varying due to moving vehicles. The first-order Markovian process is used to model the mobility of vehicles. For this system model, closed-form expressions for outage probability and system throughput are derived.

Notations: We use $F_X(\cdot)$ and $f_X(\cdot)$ to denote cumulative distribution function (CDF) and probability density function (PDF), respectively. $\mathbb{E}[\cdot]$ denotes expectation operator. $\Upsilon(\cdot,\cdot)$ represents lower incomplete Gamma function [21, eq. (8.350)] and $\Gamma(\cdot)$ denotes complete Gamma function. $\|\cdot\|$ and $|\cdot|$ denote Frobenius norm and absolute value, respectively. Further, $\triangleq$ is used to denote the equality by definition. $\mathcal{CN}(\mu,\Omega)$ represents circular complex Gaussian random variable with mean μ and variance Ω, $\mathcal{K}_v(\cdot)$ denotes vth order modified Bessel function of second kind [21, eq. (8.432)] and $\mathcal{G}_{p,q}^{m,n}\left(x\middle|\begin{matrix}b_1,\ldots,b_q\\a_1,\ldots,a_p\end{matrix}\right)$ represents the Meijer-$\mathcal{G}$ function [21, eq. (9.301)].

II. SYSTEM MODEL

As illustrated in Fig. 1, a vehicle communicates to the base station (network) with the help of multiple relay units in two phases. Here, infrastructures are converted into relays by mounting transceivers that assist the vehicles in communicating with the base station. Both vehicles and infrastructure nodes are deployed with single antenna devices and base stations with multiple antennas. All channels are considered to be independent and identically distributed (i.i.d.). In the first phase, vehicle communicates with K DF-based relays $(r_1, r_2, \ldots, r_K)$ using the RF transmission. In the second phase, hybrid FSO/RF link is employed to realize information transfer between a selected relay and the base station. Only one link (either FSO or RF) will be active at a time to enhance the system's energy efficiency. Here, the FSO link serves as a primary link, whereas the RF link is an alternative one. To exploit multiple antennas at the base station, maximum ratio combining (MRC) is considered when the RF link operates in the second phase to enhance the instantaneous SNR. Switching information between FSO and RF channels is sent using feedback bits, considering perfect channel state information. RF channels are characterized by Nakagami-m distribution, whereas FSO channel follows Rayleigh and Gamma-Gamma distribution to model pointing errors and atmospheric turbulence fading. As depicted in Fig. 2, the transmission block has time duration T, which splits into two-time slots of τT and $(1-\tau)T$ duration, where τ is the time allocation factor.

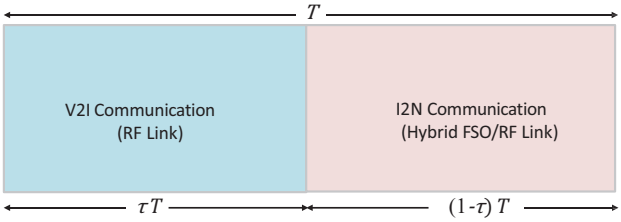

Fig. 2. Transmission block structure.

A. SNR for Vehicle-to-Infrastructure (V2I) RF Link

During the first transmission phase, vehicle transmits unit energy symbol, x_v, to all nearby infrastructure nodes. The signal received at the ith node can be expressed as

$$y_{r_i} = \sqrt{P_v} h_{v,r_i} x_v + n_{r_i}, \tag{1}$$

for $i \in \{1, 2, \ldots, K\}$, where P_v represents the transmit power at the vehicle, h_{v,r_i} is the channel gain between vehicle and infrastructure nodes and $n_{r_i} \sim \mathcal{CN}(0, \sigma_{r_i}^2)$ is the additive white Gaussian noise (AWGN). Further, we utilize first-order auto-regression process to characterize mobility of vehicle [20], [22]. Therefore, h_{v,r_i} can be modeled as

$$h_{v,r_i} = \rho \bar{h}_{v,r_i} + \sqrt{1-\rho^2} h_{e,r_i}, \tag{2}$$

where $\rho \in (0, 1]$ is correlation coefficient between h_{v,r_i} and $\bar{h}_{v,r_i}$ and can be obtained using Jake's model, i.e., $\rho = \mathcal{J}_0(\frac{2\pi f_c v_s T_d}{c})$. $\mathcal{J}_0(\cdot)$ is the zeroth-order Bessel function of first kind [21, eq.(8.402)], velocity of light in free space is denoted by c, v_s denotes relative velocity, T_d is the transmitted symbol duration and f_c is carrier frequency. The error component of channel gain is represented by $h_{e,r_i} \sim \mathcal{CN}(0, \Omega_{e,r_i})$. By substituting (2) into (1), the signal received at each relaying node is expressed as

$$y_{r_i} = \sqrt{P_v}\rho \bar{h}_{v,r_i} x_v + \sqrt{P_v(1-\rho^2)} h_{e,r_i} x_v + n_{r_i}. \tag{3}$$

Therefore, we can get instantaneous SNR at infrastructure as

$$\gamma_{v,r_i} = \frac{P_v \rho^2 |\overline{h}_{v,r_i}|^2}{P_v(1-\rho^2)\Omega_{e,r_i} + \sigma^2_{r_i}}. \quad (4)$$

B. SNR for Infrastructure-to-Network (I2N) FSO Link

During the second transmission phase, the infrastructure node having the maximum achievable SNR further transmits the signal to the base station. On utilizing the direct detection technique, the signal received via the FSO link at the base station can be given as

$$y^F_D = P_{i_F} \eta \mathcal{I}_F x_F + n_{D_F}, \quad (5)$$

where x_F represents unit energy symbol, P_{i_F} represents transmit power at the infrastructure for FSO communication, $n_{D_F} \sim \mathcal{CN}(0, \sigma^2_{D_F})$ is AWGN at the base station, η denotes optical-to-electrical power conversion factor, $\mathcal{I}_F$ is FSO link's irradiance, and is affected by pointing errors $\mathcal{I}_p$, atmospheric turbulence fading $\mathcal{I}_a$ and atmospheric attenuation $\mathcal{I}_l$. Therefore, $\mathcal{I}_F$ is mathematically represented as $\mathcal{I}_F = \mathcal{I}_a \mathcal{I}_p \mathcal{I}_l$. Using (5), we can get instantaneous SNR for FSO link at the base station as

$$\gamma^F_{r_i,D} = \frac{P^2_{i_F} \eta^2 \mathcal{I}^2_F}{\sigma^2_{D_F}}, \quad (6)$$

and the FSO link's average electrical SNR as

$$\overline{\gamma}^F_{r_i,D} = \frac{P^2_{i_F} \eta^2 (\mathbb{E}[\mathcal{I}_F])^2}{\sigma^2_{D_F}}. \quad (7)$$

C. SNR for I2N RF Link

As base station is deployed with N number of antennas, N signal copies are received at the destination through the RF link. Therefore, MRC technique is performed on the received signals with weight vectors, i.e., $w^T_{r_i} = \frac{h^\dagger_{r_i,D}}{\|h_{r_i,D}\|}$. At the destination, the overall received signal can be expressed as

$$y^{RF}_{r_i,D} = \sqrt{P_{i_{RF}}} \|h_{r_i,D}\| x_v + \tilde{n}_D, \quad (8)$$

where $\|h_{r_i,D}\| = \sqrt{|h^1_{r_i,D}|^2 + |h^2_{r_i,D}|^2 + ... + |h^N_{r_i,D}|^2}$ is the channel gain, $P_{i_{RF}}$ represents transmit power for RF transmission at the infrastructure, and $\tilde{n}_D = w^T_{r_i} n_D \sim \mathcal{CN}(0, \sigma^2_D)$ is AWGN. Hereby, the instantaneous SNR is given as

$$\gamma^{RF}_{r_i,D} = \frac{P_{i_{RF}} \|h_{r_i,D}\|^2}{\sigma^2_D}. \quad (9)$$

D. CDF of V2I RF link

For RF links, all channels are assumed to follow the Nakagami-m distribution. Hence, channel gain $|\overline{h}_{v,r_i}|^2$ follows Gamma distribution. Therefore, we can have the corresponding CDF of RF link as

$$F_{\gamma_{v,r_i}}(x) = \Pr[\gamma_{v,r_i} \leq x]. \quad (10)$$

Using (4) and [21, eq. (8.350)], the CDF can be expressed as

$$F_{\gamma_{v,r_i}}(x) = \frac{1}{\Gamma(m_{vi})} \Upsilon \left[m_{vi}, \frac{m_{vi} P_v (1-\rho^2) \Omega_{e,r_i} x + \sigma^2_{r_i}}{\Omega_{vi} P_v \rho^2} \right], \quad (11)$$

where $x \geq 0$, $m_{vi} \geq 1/2$ is Nakagami-m fading severity parameter. Here vehicle communicates with multiple relays, i.e., r_i, for $i = 1, 2, \ldots, K$. Therefore, best relay is selected to further transmit information to the base station based on the following criteria

$$\gamma^*_{v,r_i} = \max_{i \in \{1,2,\ldots,K\}} (\gamma_{v,r_i}). \quad (12)$$

The CDF of instantaneous SNR in the first phase corresponding to best relay is given as

$$F_{\gamma^*_{v,r_i}}(x) = \Pr[\max(\gamma_{v,r_i}) \leq x] = \prod_{i=1}^{K} \Pr[\gamma_{v,r_i} \leq x]. \quad (13)$$

All the channels are i.i.d., the CDF can be expressed as

$$F_{\gamma^*_{v,r_i}}(x) = (F_{\gamma_{v,r_i}}(x))^K. \quad (14)$$

E. CDF of I2N RF Link

As the base station is installed with N antennas, MRC technique is utilized to maximize the instantaneous SNR. The PDF of $\gamma^{RF}_{r_i,D}$ can be expressed as [23]

$$f_{\gamma^{RF}_{r_i,D}}(y) = \frac{y^{m_{iD}N-1}}{\Gamma(m_{iD}N)} \left(\frac{m_{iD}}{\Omega_{iD}} \right)^{m_{iD}N} \exp\left(\frac{-m_{iD} y}{\Omega_{iD}} \right), y \geq 0, \quad (15)$$

where Ω_{iD} is the average SNR, and $m_{iD} \geq 1/2$ is Nakagami fading parameter. The corresponding CDF of $\gamma^{RF}_{r_i,D}$ can be given as

$$F_{\gamma^{RF}_{r_i,D}}(y) = \frac{1}{\Gamma(m_{iD}N)} \Upsilon \left[m_{iD}N, \frac{m_{iD} y}{\Omega_{iD}} \right], y \geq 0. \quad (16)$$

F. CDF of I2N FSO Link

The fluctuations in the irradiance of FSO link is due to $\mathcal{I}_a$, $\mathcal{I}_p$ and $\mathcal{I}_l$. Therefore, composite irradiance $\mathcal{I}_F$ can be given as $\mathcal{I}_F = \mathcal{I}_a \mathcal{I}_p \mathcal{I}_l$. Let $\mathcal{I}_a$ is characterized by Gamma-Gamma distribution, which can be obtained by finding the product of two independent Gamma distributions, i.e. $\mathcal{I}_a = XY$. Here, large-scale and small-scale turbulence impacts are represented by X and Y, respectively. Therefore, PDFs of X and Y are given as $f_X(x) = \frac{\alpha^\alpha}{\Gamma(\alpha)} x^{\alpha-1} e^{-\alpha x}, x \geq 0, \alpha > 0$, and $f_Y(y) = \frac{\beta^\beta}{\Gamma(\beta)} y^{\beta-1} e^{-\beta y}, y \geq 0, \beta > 0$, respectively. To evaluate the CDF of $\mathcal{I}_a$, we define the following function as $F_{\mathcal{I}_a}(i_a) = \Pr[XY \leq i_a]$ and its integral forms is given as

$$F_{\mathcal{I}_a}(i_a) = \int_0^\infty \int_0^{\frac{i_a}{x}} f_X(x) f_Y(y) dx dy. \quad (17)$$

Further, differentiating both sides w.r.t. i_a and considering $y = \frac{i_a}{x}$ and utilizing [21, eq.(3.471.9)], we can have the PDF of $\mathcal{I}_a$ as

$$f_{\mathcal{I}_a}(i_a) = \frac{2(\alpha\beta)^{\frac{\alpha+\beta}{2}}}{\Gamma(\alpha)\Gamma(\beta)} i_a^{\frac{\alpha+\beta}{2}-1} \mathcal{K}_{\alpha-\beta}(2\sqrt{\alpha\beta i_a}). \quad (18)$$

Furthermore, using the transformation $\mathcal{K}_v(x) = \frac{1}{2} \mathcal{G}^{2,0}_{0,2} \left(\frac{x^2}{4} \middle| \frac{v}{2}, \frac{-v}{2} \right)$ [24, eqs. (03.04.26.0008.01), (07.34.21.0084.01)], we can have the CDF expression of $\mathcal{I}_a$ as

$$F_{\mathcal{I}_a}(i_a) = \frac{(\alpha\beta)^{\frac{\alpha+\beta}{2}}}{\Gamma(\alpha)\Gamma(\beta)} i_a^{\frac{\alpha+\beta}{2}} \mathcal{G}^{1,3}_{2,1} \left(\alpha\beta i_a \middle| \begin{matrix} \frac{2-\alpha-\beta}{2} \\ \frac{\alpha-\beta}{2}, -\frac{\alpha-\beta}{2}, \frac{-\alpha-\beta}{2} \end{matrix} \right), \quad (19)$$

where α and β represent small scale and large scale parameters of the scattering environment, respectively. Now, attenuation due to geometric spread with detector's radius r and pointing error ξ is expressed as [25]

$$\mathcal{I}_p(\xi, l) \approx A_0 \exp\left(-\frac{2\xi^2}{w_{leq}^2}\right), \tag{20}$$

where A_0 is the fraction of the power collected at $\xi = 0$, w_{leq} is equivalent beam width related as $w_{leq}^2 = \frac{w_l^2 \pi \text{erf}(v)}{2ve^{-v^2}}$ with $v = \frac{\sqrt{\pi}r}{\sqrt{2}w_l}$ and $A_0 = \text{erf}(v^2)$. Further, $w_l \approx w_0\sqrt{1+\epsilon\left(\frac{\lambda l}{\pi w_0^2}\right)^2}$, where l is FSO link distance. At $l = 0$, $w_l \approx w_0$, w_0 denotes beam radius of beam waist. Also, $\epsilon = 1 + \frac{2w_0^2}{\rho_0(l)^2}$, where $\rho_0(l)$ is the coherence radius given as $\rho_0(l) = (0.55C_n^2k^2l)^{-3/5}$, where $k = \frac{2\pi}{\lambda}$ represents wave number and C_n^2 denotes refractive index parameter. Further, the sum of elevation and horizontal displacements is used to express pointing error ξ, assuming them to follow independent Gaussian distributions, Therefore, ξ will be modeled as Rayleigh distribution and the PDF is given as

$$f_\xi(\xi) = \frac{\xi}{\sigma_s^2} \exp^{-\frac{\xi^2}{2\sigma_s^2}},\ \xi \geq 0, \tag{21}$$

where σ_s^2 is displacement variance of pointing error. By combining (20) and (21) with variable transformation, we can have PDF of $\mathcal{I}_p$ as

$$f_{\mathcal{I}_p}(i_p) = \frac{z^2}{A_0^{z^2}} i_p^{z^2-1}, \tag{22}$$

for $0 \leq i_p \leq A_0$ and $z \triangleq \frac{w_{leq}}{2\sigma_s}$. Further, by using relation $F_{\mathcal{I}_p}(i_p) = \int_0^{i_p} f_{\mathcal{I}_p}(i_p)di_p$, we can have the CDF of $\mathcal{I}_p$ as

$$F_{\mathcal{I}_p}(i_p) = \left(\frac{i_p}{A_0}\right)^{z^2}. \tag{23}$$

By using Beer-Lambert's law [25], attenuation factor can be determined as

$$\mathcal{I}_l = \frac{P(\lambda, L)}{P(\lambda, 0)} = \exp(-\Xi(\lambda)), \tag{24}$$

where $P(\lambda, 0)$ is power emitted by source, $P(\lambda, L)$ is signal power at distance L, and λ is wavelength of the signal. $\Xi(\lambda)$ is extinction coefficient, and can be expressed as sum of absorption coefficients and scattering.

Further, the expressions for CDF and PDF of $\mathcal{I}_F$ is formulated, using relation $\mathcal{I}_F = \mathcal{I}_a\mathcal{I}_p\mathcal{I}_l$. Here, $\mathcal{I}_l$ is considered to be deterministic. Therefore, we can have PDF of $\mathcal{I}_F$ in an integral form as

$$f_{\mathcal{I}_F}(i_F) = \int_0^\infty f_{\mathcal{I}_a}(i_a) f_{\mathcal{I}_p}\left(\frac{1}{i_a\mathcal{I}_l}\right) di_a. \tag{25}$$

From (22), $\mathcal{I}_p$ can take values from 0 to A_0, therefore, limits for i_a is from $0 \leq \frac{i_F}{i_a\mathcal{I}_l} \leq A_0$, i.e., $i_a \geq \frac{i_F}{A_0\mathcal{I}_l}$. By taking boundaries of i_a and PDFs of $\mathcal{I}_p$ and $\mathcal{I}_a$ in (25), the PDF of $\mathcal{I}_F$ can be obtained as

$$f_{I_F}(i_F) = \frac{2\xi^2(\alpha\beta)^{\frac{\alpha+\beta}{2}}}{\Gamma(\alpha)\Gamma(\beta)} \frac{i_F^{\xi^2-1}}{\mathcal{I}_l^{\xi^2} A_0^{\xi^2}} \int_{\frac{i_F}{A_0\mathcal{I}_l}}^\infty i_a^{\frac{\alpha+\beta}{2}-\xi^2-1} \times \mathcal{K}_{\alpha-\beta}\left(2\sqrt{\alpha\beta i_a}\right) di_a. \tag{26}$$

By utilizing [24, eqs.(03.04.26.0008.01), (07.34.21.0085.01)] in (26), the PDF of $\mathcal{I}_F$ can be given as

$$f_{\mathcal{I}_F}(i_F) = \frac{\xi^2}{\Gamma(\alpha)\Gamma(\beta)} \left(\frac{\alpha\beta}{A_0\mathcal{I}_l}\right)^{\frac{\alpha+\beta}{2}} i_F^{\frac{\alpha+\beta}{2}-1} \times \mathcal{G}_{1,3}^{3,0}\left(\frac{\alpha\beta i_F}{A_0\mathcal{I}_l}\middle| \begin{matrix}\xi^2-\frac{\alpha+\beta}{2}+1 \\ \xi^2-\frac{\alpha+\beta}{2}, \frac{\alpha-\beta}{2}, \frac{\alpha+\beta}{2}\end{matrix}\right). \tag{27}$$

Further, by integrating (27) and using [24, eq.(07.34.21.0084.01)], and [21, eq.(9.31.5)], we can have the CDF of $\mathcal{I}_F$ as

$$F_{\mathcal{I}_F}(i_F) = \frac{\xi^2}{\Gamma(\alpha)\Gamma(\beta)} \mathcal{G}_{2,4}^{3,1}\left(\frac{\alpha\beta i_F}{A_0\mathcal{I}_l}\middle| \begin{matrix}1, \xi^2+1 \\ \xi^2, \alpha, \beta, 0\end{matrix}\right). \tag{28}$$

On performing some algebraic transformations in (28), the CDF of the FSO link can be derived as

$$F_{\gamma_{r_i,D}^F}(x) = \frac{\xi^2}{\Gamma(\alpha)\Gamma(\beta)} \mathcal{G}_{2,4}^{3,1}\left(\alpha\beta h\sqrt{\frac{x}{\overline{\gamma}_{r_i,D}^F}}\middle| \begin{matrix}1, \xi^2+1 \\ \xi^2, \alpha, \beta, 0\end{matrix}\right), \tag{29}$$

where $h = \frac{\xi^2}{\xi^2+1}$.

III. Performance Analysis

A. Outage Probability

The system will be considered in an outage if the infrastructure node or the base station fails to achieve the required target rate using the available resources in the first and second phases, respectively. Thereby, the OP expression can be mathematically expressed as

$$\begin{aligned}\mathcal{P}_{\text{out}} &= 1 - \Pr[\mathcal{R}_{v,r_i} > r_{\text{th}}]\Pr[\max(\mathcal{R}_{r_i,D}^F, \mathcal{R}_{r_i,D}^{RF}) > r_{\text{th}}] \\ &= 1 - (1 - \Pr[\gamma_{v,r_i} \leq \varphi_i])(1 - \Pr[\gamma_D \leq \varphi_D]) \\ &= F_{\gamma_{v,r_i}}(\varphi_i) + F_{\gamma_D}(\varphi_D) - F_{\gamma_{v,r_i}}(\varphi_i)F_{\gamma_D}(\varphi_D),\end{aligned} \tag{30}$$

where $\mathcal{R}_{v,r_i} = \tau\log_2(1+\gamma_{v,r_i})$, $\mathcal{R}_{r_i,D}^F = (1-\tau)\log_2(1+\gamma_{r_i,D}^F)$, and $\mathcal{R}_{r_i,D}^{RF} = (1-\tau)\log_2(1+\gamma_{r_i,D}^{RF})$ are the instantaneous achievable rates at the infrastructure node and the base station. Further, $\varphi_i = 2^{\frac{r_{\text{th}}}{\tau}} - 1$ is threshold SNR at relay units for RF link and $\varphi_D = 2^{\frac{r_{\text{th}}}{1-\tau}} - 1$ represents threshold SNR at the base station. During the second phase, information is transmitted to the base station by utilizing hybrid FSO/RF transmission. Herein, FSO acts as a primary link and continues to transmit until its instantaneous SNR, i.e., $\gamma_{r_i,D}^F$ is higher than a predefined threshold value (φ_D). If the instantaneous SNR falls below φ_D, FSO link will be deactivated and the backup RF link will be activated. Therefore, hybrid FSO/RF link is in outage when the received SNR of both FSO and RF links falls below φ_D. The expression of $F_{\gamma_D}(\varphi_D)$ for hybrid FSO/RF link can be given as

$$\begin{aligned}F_{\gamma_D}(\varphi_D) &= \Pr[\gamma_{r_i,D}^F \leq \varphi_D]\Pr[\gamma_{r_i,D}^{RF} \leq \varphi_D] \\ &= F_{\gamma_{r_i,D}^F}(\varphi_D)F_{\gamma_{r_i,D}^{RF}}(\varphi_D).\end{aligned} \tag{31}$$

By substituting (16) and (29) in (31), we can get the expression of OP the of hybrid FSO/RF sub-system. Hence, substituting (14), and (31) in (30), we can obtain the OP of

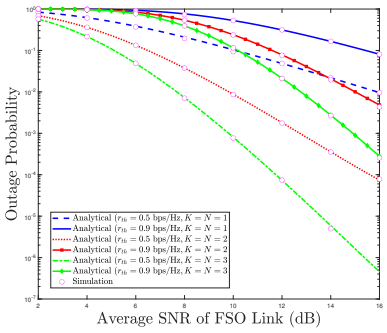

Fig. 3. OP vs. SNR for different $r_{\rm th}$.

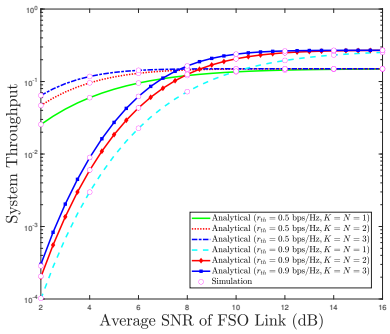

Fig. 4. ST vs. SNR for different $r_{\rm th}$.

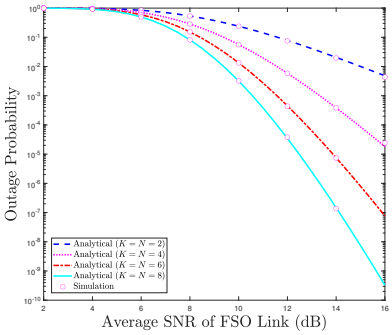

Fig. 5. OP vs. SNR for different K and N.

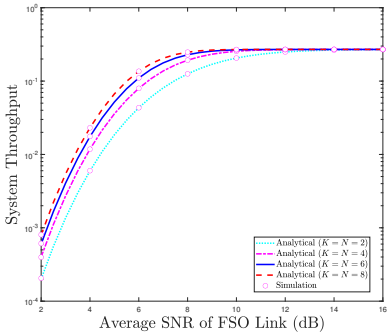

Fig. 6. ST vs. SNR for different K and N.

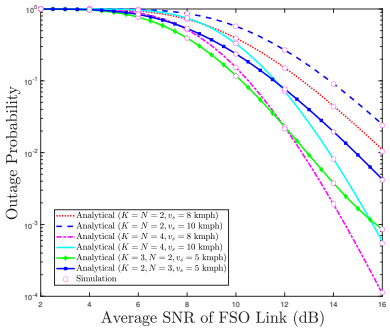

Fig. 7. OP vs. SNR for different v_s.

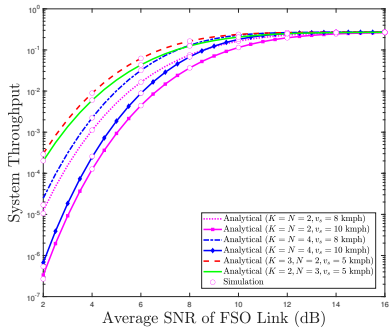

Fig. 8. ST vs. SNR for different v_s.

the system as

$$
\begin{aligned}
P_{\rm out} = &\left(\frac{1}{\Gamma(m_{vi})}\Upsilon\left[m_{vi}, \frac{m_{vi}\varphi_i P_v(1-\rho^2)\Omega_{e,r_i}+\sigma_{r_i}^2}{\Omega_{vi}P_v\rho^2}\right]\right)^K \\
&+\left(\frac{1}{\Gamma(m_{iD}N)}\Upsilon\left[m_{iD}N, \frac{m_{iD}\varphi_D}{\Omega_{iD}}\right]\right) \\
&\times\left(\frac{\xi^2}{\Gamma(\alpha)\Gamma(\beta)}\mathcal{G}_{2,4}^{3,1}\left(\alpha\beta h\sqrt{\frac{\varphi_D}{\overline{\gamma}_{r_i,D}^F}}\middle|\begin{matrix}1,\xi^2+1\\ \xi^2,\alpha,\beta,0\end{matrix}\right)\right) \\
&-\left(\frac{1}{\Gamma(m_{vi})}\Upsilon\left[m_{vi}, \frac{m_{vi}\varphi_i P_v(1-\rho^2)\Omega_{e,r_i}+\sigma_{r_i}^2}{\Omega_{vi}P_v\rho^2}\right]\right)^K \\
&\times\left(\frac{1}{\Gamma(m_{iD}N)}\Upsilon\left[m_{iD}N, \frac{m_{iD}\varphi_D}{\Omega_{iD}}\right]\right) \\
&\times\left(\frac{\xi^2}{\Gamma(\alpha)\Gamma(\beta)}\mathcal{G}_{2,4}^{3,1}\left(\alpha\beta h\sqrt{\frac{\varphi_D}{\overline{\gamma}_{r_i,D}^F}}\middle|\begin{matrix}1,\xi^2+1\\ \xi^2,\alpha,\beta,0\end{matrix}\right)\right). \qquad (32)
\end{aligned}
$$

B. System Throughput (ST)

By assuming a delay-limited scenario, the system throughput can be defined using threshold data rate and OP, as [26]

$$\mathcal{S}_T = \min\left[\tau(1-\Pr[\gamma_{v,r_i}\le\varphi_i])r_{\rm th}, (1-\tau)(1-\Pr[\gamma_D\le\varphi_D])r_{\rm th}\right]. \qquad (33)$$

By utilizing (14), and (31) in (33), we can obtain the expression for system throughput.

IV. Numerical Results

For getting numerical and simulation results, we set the following parameters as $m_{vi}=m_{iD}=2$, $\Omega_{vi}=\Omega_{iD}=1$, $\alpha=5.41$, $\beta=3.78$, $P_{i_{RF}}=80$mW, $T_d=1$ms, $f_c=1.9$ GHz, $c=3X10^8$, $\sigma_{r_i}^2=1$ dBm, $\Omega_{e,r_i}=0.5$ dBm, $\lambda=1550$ cm, $C_n^2=10^{-13}$, $w_0=5$ cm, $l=1000$ m, $r=14$ cm, $\sigma_s=10$ cm, and $\tau=0.3$ and used $\overline{\gamma}_{r_i,D}^F$ as average SNR. In Figs. 3 and 4, we plot OP and system throughput versus average SNR curves for different target rates, respectively, assuming $P_v=20$ dB and $v_s=5$ kmph. From Fig. 3, we can observe that the outage performance degrades as the target data rate increases for the considered parameters. This behavior of the OP is expected because the instantaneous rates that may be attained at the base station tend to fall below the target threshold when the target rate increases with a fixed average SNR value, resulting in higher OP. Also, when we increase the average SNR value, OP decreases due to a higher achievable instantaneous rate at the base station.

Fig. 4 shows that the system throughput's value is considerably lower for lower average SNR values because the instantaneous SNR attained would be significantly less than the target SNR, resulting in higher OP. Moreover, when average SNR increases, system throughput improves to a certain level before reaching saturation. As a result, the system performs better with higher average SNR levels. The system throughput improvement attains its maximum value corresponding to the target rate when the average SNR exceeds a specific value. This saturated system throughput value can be considered as the maximum achievable throughput with that set of parameters. Furthermore, the performance of proposed system is compared with a single antenna and single relay based hybrid FSO/RF system in terms of OP and system throughput. From these figures, it is evident that the considered system outperforms such systems as MRC is employed at the base station, increasing the channel gain and multiple relay improve the OP performance

in the first phase.

Figs. 5 and 6 show the OP and system throughput curves versus average SNR values with the different number of receiving antennas at the base station and considering $P_v = 20$ dB, $v_s = 5$ kmph, and $r_{\text{th}} = 0.9$ bps/Hz. It can be observed from Fig. 5 that the increase in the number of receiving antennas results in an increase in diversity order, and hence the OP degrades. With MRC at the base station, the channel gain increases significantly, therefore, offering better OP performance. In Fig. 6, it can be observed that at lower average SNR values, system throughput improves with an increase in receiving antennas because the probability that the system experiences outage decreases. However, beyond the specified value of the acquired throughput, no more improvement in the system throughput can be obtained with an increase in average SNR.

In Figs. 7 and 8, we demonstrate the OP and system throughput performance with varying average SNR for different values of relative speed, i.e., v_s. Fig. 7 shows that OP degrades with the increase in average SNR, whereas Fig. 8 highlights that system throughput increases for a considered set of parameters, i.e., $P_v = 20$ dB, and $r_{\text{th}} = 0.9$ bps/Hz. It can also be depicted from these figures that at the same relative velocity by increasing the number of receiving antennas at the base station, the system performance improves as the gain of the channel increases by using MRC receiver. Moreover, one can notice that the system performance degrades with the increase in the relative velocity considering the same number of receiving antennas.

V. Conclusion

This paper has investigated the performance of the proposed system that uses multiple transceiver-mounted roadside infrastructures to ease the communication between vehicles to the network. Herein, we have considered vehicles and infrastructures with single antennas, whereas multiple antennas are deployed at the base station. RF link is modeled by Nakagami-m distribution, whereas FSO link experiences Gamma-Gamma distribution. To increase communication reliability, an RF link acts as an alternative for FSO transmission, which offers high data rates. We have taken a realistic scenario by including atmospheric attenuation, Rayleigh distributed pointing errors, and Gamma-Gamma distributed atmospheric fading, which may severely affect the FSO link's performance. At the base station, received RF signals are combined using MRC, which improves the system performance. The OP and system throughput expressions are derived for analyzing the performance. Simulation results are included to verify that all derived analytical findings are accurate.

References

[1] H. Peng, L. Liang, X. Shen, and G. Y. Li, "Vehicular communications: A network layer perspective," *IEEE Trans. Vehicular Technol.*, vol. 68, no. 2, pp. 1064–1078, 2019.

[2] H. Zhou, W. Xu, J. Chen, and W. Wang, "Evolutionary V2X technologies toward the Internet of vehicles: Challenges and opportunities," *Proceedings of the IEEE*, vol. 108, no. 2, pp. 308–323, 2020.

[3] L. Miao, S.-F. Chen, Y.-L. Hsu, and K.-L. Hua, "How does C-V2X help autonomous driving to avoid accidents?" *Sensors*, vol. 22, no. 2, p. 686, Jan 2022. [Online]. Available: http://dx.doi.org/10.3390/s22020686

[4] B. Ji, X. Zhang, S. Mumtaz, C. Han, C. Li, H. Wen, and D. Wang, "Survey on the internet of vehicles: Network architectures and applications," *IEEE Commun. Standards Mag.*, vol. 4, no. 1, pp. 34–41, 2020.

[5] H. Harald, E. Jaafar, and W. Ian, "Optical wireless communication," *Phil. Trans. R. Soc. A*, vol. 378, no. 2169, pp. 1–11, 2020.

[6] E. Balti, M. Guizani, B. Hamdaoui, and B. Khalfi, "Aggregate hardware impairments over mixed RF/FSO relaying systems with outdated CSI," *IEEE Trans. Commun.*, vol. 66, no. 3, pp. 1110–1123, 2018.

[7] I. K. Son and S. Mao, "A survey of free space optical networks," *Digital Commun. & Networks*, vol. 3, no. 2, pp. 67–77, 2017.

[8] M. Z. Chowdhury, M. Shahjalal, S. Ahmed, and Y. M. Jang, "6G wireless communication systems: Applications, requirements, technologies, challenges, and research directions," *IEEE Open J. Communications Society*, vol. 1, pp. 957–975, 2020.

[9] E. Lee, J. Park, D. Han, and G. Yoon, "Performance analysis of the asymmetric dual-hop relay transmission with mixed RF/FSO links," *IEEE Photonics Technol. Lett.*, vol. 23, no. 21, pp. 1642–1644, 2011.

[10] M. Petkovic, G. T. Djordjevic, and I. B. Djordjevic, "Analysis of mixed RF/FSO system with imperfect CSI estimation," in *2017 19th International Conference on Transparent Optical Networks (ICTON)*, 2017, pp. 1–7.

[11] H. Lei, Z. Dai, K.-H. Park, W. Lei, G. Pan, and M.-S. Alouini, "Secrecy outage analysis of mixed RF-FSO downlink SWIPT systems," *IEEE Trans. Commun.*, vol. 66, no. 12, pp. 6384–6395, 2018.

[12] I. Ahamed and M. Vijay, "Comparison of different diversity techniques in MIMO antennas," in *2017 2nd International Conference on Communication and Electronics Systems (ICCES)*, 2017, pp. 47–50.

[13] H. Liang, C. Gao, Y. Li, M. Miao, and X. Li, "Analysis of selection combining scheme for hybrid FSO/RF transmission considering misalignment," *Optics Communications*, vol. 435, pp. 399–404, 2019.

[14] N. Vishwakarma and S. R, "Performance analysis of hybrid FSO/RF communication over generalized fading models," *Optics Communications*, vol. 487, p. 126796, 2021.

[15] E. Lee, J. Park, D. Han, and G. Yoon, "Performance analysis of the asymmetric dual-hop relay transmission with mixed RF/FSO links," *IEEE Photonics Technol. Lett.*, vol. 23, no. 21, pp. 1642–1644, 2011.

[16] M. Petkovic, G. T. Djordjevic, and I. B. Djordjevic, "Analysis of mixed RF/FSO system with imperfect CSI estimation," in *2017 19th International Conference on Transparent Optical Networks (ICTON)*, 2017, pp. 1–7.

[17] M. A. Amirabadi and V. Tabataba Vakili, "Performance of a relay-assisted hybrid FSO/RF communication system," *Physical Communication*, vol. 35, p. 100729, 2019.

[18] J. Zhang, H. Ran, X. Pan, G. Pan, and Y. Xie, "Outage analysis of wireless-powered relaying FSO-RF systems with nonlinear energy harvesting," *Optics Communications*, vol. 477, p. 126309, 2020.

[19] A. K. Meshram, D. S. Gurjar, and P. K. Upadhyay, "Joint impact of nodes-mobility and channel estimation error on the performance of two-way relay systems," *Physical Communication*, vol. 23, pp. 103–113, 2017.

[20] A. Pandey and S. Yadav, "Joint impact of nodes mobility and imperfect channel estimates on the secrecy performance of cognitive radio vehicular networks over nakagami-m fading channels," *IEEE Open J. Veh. Technol.*, vol. 2, pp. 289–309, 2021.

[21] I. Gradshteyn and I. Ryzhik, *Table of Integrals, Series, and Product.Cambridge, MA, USA: Academic press*, 2014.

[22] N. Varshney and P. Puri, "Performance analysis of decode-and-forward-based mixed MIMO-RF/FSO cooperative systems with source mobility and imperfect CSI," *Journal of Lightwave Technology*, vol. 35, no. 11, pp. 2070–2077, 2017.

[23] E. K. Al-Hussaini and A. A. M. Al-Bassiouni, "Performance of MRC diversity systems for the detection of signals with nakagami fading," *IEEE Trans. Commun.*, vol. 33, pp. 1315–1319, 1985.

[24] The wolfram functions site. [Online]. Available: http://functions.wolfram.com/

[25] S. Sharma, A. S. Madhukumar, and R. Swaminathan, "Effect of pointing errors on the performance of hybrid FSO/RF networks," *IEEE Access*, vol. 7, pp. 131 418–131 434, 2019.

[26] M. Hossain, P. Vitthaladevuni, M.-S. Alouini, V. Bhargava, and A. Goldsmith, "Adaptive hierarchical modulation for simultaneous voice and multiclass data transmission over fading channels," *IEEE Trans. Veh. Technol.*, vol. 55, no. 4, pp. 1181–1194, 2006.